Tao *et al. Biochar* (2026) 8:116
https://doi.org/10.1007/s42773-026-00629-5

Biochar

ORIGINAL RESEARCH Open Access

Effect of initial water content on the pyrolysis mechanism of lignocellulosic biomass

Wenmei Tao[1,2], Linjian Gao[1], Mengzi Li[1], Yunzhu Wang[3], Lin Shi[4], Chengcheng Xu[1], Xinyuan Lu[1] and Bo Pan[2*]

Abstract

The initial water content in lignocellulosic biomass significantly influences the pyrolysis process, but the effect of the form of water, especially free water (FW) and bound water (BW), remains unclear. In this study, the pyrolytic characteristics of cellulose (CL), lignin (LG), and rice straw (RS) with different initial water contents were investigated using TG, TG-DSC, TG-MS, and in situ FTIR. The results showed that both FW and BW decreased the maximum thermal decomposition rate and increased the biochar yield. The activation energy of hemicellulose (*E*-HC) linearly decreased upon increasing the BW content ($r = -0.90$, $p < 0.05$). Combined two-dimensional FTIR correlation spectroscopy (2D-FTIR-COS) and TG-MS analyses showed that BW formed hydrogen bonds with O-acetyl groups in HC, accelerating its decomposition and the release of CH_3COOH at lower temperatures. In contrast, a significant positive correlation was found between BW and the activation energy of cellulose (*E*-CL) due to the hydrogen bond network generated between BW and CL. The 2D-FTIR-COS spectra revealed that the primary sequential water responses of functional groups during RS pyrolysis followed the order: hydroxyl –OH → carboxyl C = O → aliphatic C–H → carbohydrate C–O–C → aromatic rings. This order shows that water promoted biochar formation, especially for biomass with higher lignin contents. The establishment of this relationship between water and pyrolysis products provides an important basis for regulating the water content during biomass pyrolysis.

Highlights

- Water promotes biochar formation by slowing the pyrolysis reaction rate.
- Bound water decreases the activation energy of hemicellulose.
- Bound water increases the activation energy of cellulose.

Keywords Lignocellulosic biomass, Pyrolysis, Bound water, Free water, Biochar yield

*Correspondence:
Bo Pan
panbocai@gmail.com
Full list of author information is available at the end of the article

Springer

Graphical Abstract

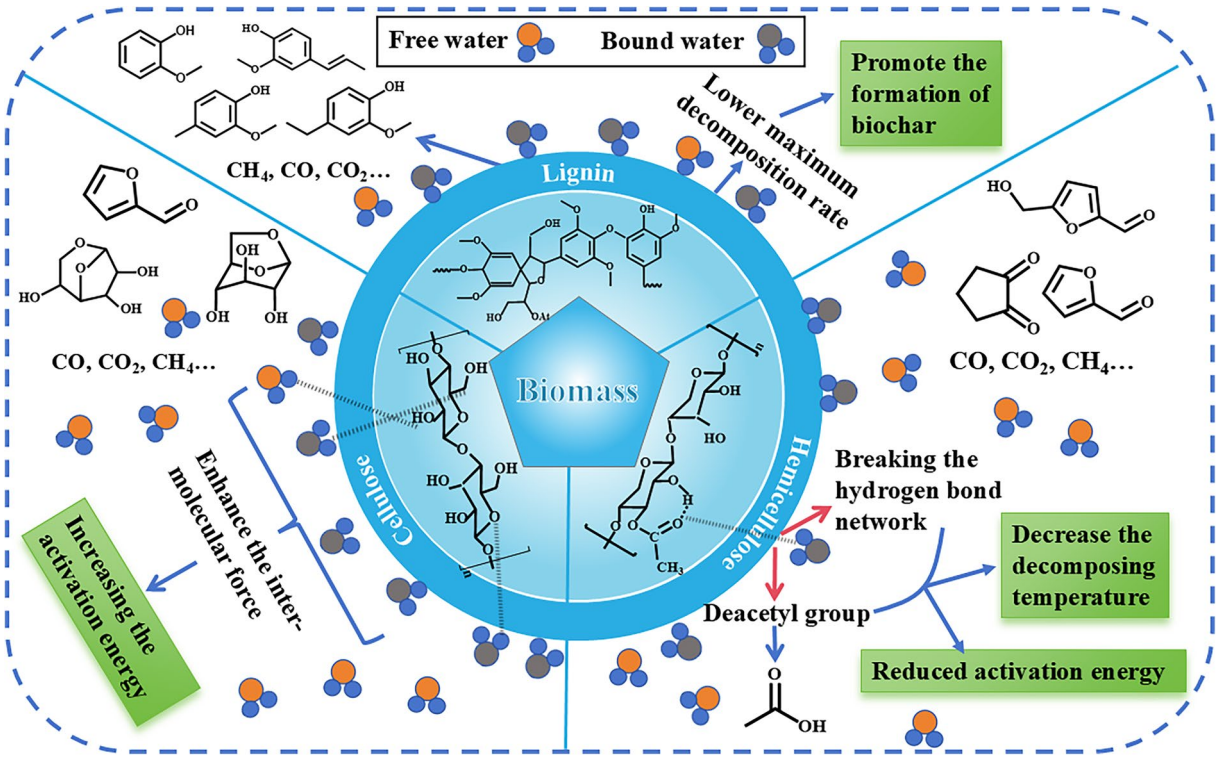

1 Introduction

Pyrolysis produces economically valuable products such as biogas, bio-oil, and biochar from biomass (Velden et al. 2010). Most studies have focused on dry biomass (Pang and Mujumdar 2010), but natural biomass usually has a high water content ranging from 25% to 60% (Carpenter et al. 2014). For example, freshly harvested corn stover has a water content exceeding 45% (Shinners et al. 2007). The initial water influences the pyrolysis process due to its large specific heat capacity, which affects heat transfer during pyrolysis (Yang et al. 2020). Water evaporation from biomass pellets may decrease the pyrolysis temperature by consuming heat. For example, wood with an initial water content of 40% requires an additional 1120 kJ kg^{-1} of energy to initiate the pyrolysis reaction compared with a dry wood sample (Akhtar and Amin 2012). Water evaporation consumes significant amounts of latent heat during pyrolysis, so high-water feedstocks might decrease the heating rate and raise the overall energy demand during pyrolysis. The released water vapor may promotes the decomposition of volatiles and reacts with the char surface, further altering the structure and properties of the resulting char. Water vapor may also participate in intermolecular hydrolysis and esterification reactions of volatiles (Gao et al. 2022). Water can narrow the temperature range of biopolymer decomposition and accelerate the volatilization rate during the pyrolysis of pine needles, decayed leaves, and peat mosses. Additionally, compared with the dry biomass, water increases the oxygen content of bio-oil and shifts the product distribution away from biochar to biooil during cellulose pyrolysis. Moreover, the reaction between water vapor and char may accelerate the cleavage of oxygen-containing functional groups such as hydroxy and carboxyl groups (Luo et al. 2023). Although it is well-established that initial water in biomass indeed participates in pyrolysis reactions, it is unclear how the form of water, i.e., free water (FW) and bound water (BW), affects pyrolysis reactions. Thus, detailed research on biomass pyrolysis with different initial water types is needed.

Water in biomass is mainly present as FW and BW. FW refers to water that is not hydrogen-bonded to a polymer, while BW is hydrogen-bonded to biopolymers such as cellulose, hemicellulose, or lignin. During the initial stage of pyrolysis, the evaporation of FW requires the absorption of heat, which may significantly reduce the initial

pyrolysis reaction rate (Jerzak et al. 2022). FW can be removed in oven by drying at 90 °C for 48 h (Wang et al. 2025). It can be inferred that FW does not participate in the subsequent pyrolysis reactions. Unlike the easily thermally evaporated FW, BW may act as a thermal buffer by forming hydrogen bonds with polymers, thereby delaying the onset of pyrolysis at lower temperatures (Paajanen et al. 2019). The dissociation of BW may change the distribution of thermal energy and accelerate the cleavage of lignin and hemicellulose via hydration (Zhao et al. 2023). By promoting aromatization reactions in biochar, BW may enhance the structural stability and yield of biochar (Chen et al. 2022a). No consensus has been reached in terms of how FW and BW interact and affect biomass (Bikbulatova et al. 2018; Nwaka et al. 2016). Although previous studies have observed that water affects biomass pyrolysis and promotes the release of gaseous products (H_2, CO, CO_2, and CH_4) (Liu et al. 2014), these results were generally obtained by a simple analysis of only a few data points. This limits the reliability of any proposed interactions between water and cellulose, hemicellulose, and lignin. Therefore, it is necessary to investigate the mechanism by which water influences pyrolysis via online characterization.

In this study, the online pyrolytic characteristics of cellulose (CL), lignin (LG), and rice straw (RS) with different initial water contents were investigated using TG, TG-DSC, TG-MS, and In situ drift FTIR. The activation energy E was calculated using the Coats-Redfern method to investigate the effects of FW and BW on pyrolysis. In situ drift FTIR was used for the online characterization of water-induced changes in functional groups. Subtle variations, directions, and sequential water responses of functional groups during pyrolysis were evaluated using two-dimensional correlation spectroscopy (2D-COS). Finally, a molecular-level water-response mechanism of biomass pyrolysis was proposed. This study provides new insights into how to regulate water-oriented pyrolysis products and closes a theoretical gap in how to pyrolyze wet biomass.

2 Materials and methods

2.1 Materials

RS samples were collected from a local agricultural farm in Yunnan, China and then sieved through a 100-mesh sieve after thorough milling. CL and LG samples were purchased from Aladdin. CL, LG, and RS samples were first submerged in deionized water and then dried in a vacuum oven by controlling the residence time to produce samples with different water contents. Hemicellulose samples with different water contents were omitted because hemicellulose can clump tightly after absorbing water, making it difficult to disperse into powder for DSC, TG, and in situ drift FTIR characterization. The water and ash contents were determined following the procedure outlined in ASTM Standards E1756-08 and E1755-01, respectively. The cellulose and hemicellulose contents of biomass were determined by the NREL method (Sluiter et al. 2008). The lignin content was determined by Klason's method. The proximate analysis, elemental analysis, and biochemical analysis results are presented in Table S1.

2.2 Low-temperature differential scanning calorimetry (DSC)

Low-temperature differential scanning calorimetry (DSC 214 Polyma, NETZSCH, Germany) was used to investigate the water distribution in CL, LG, and RS samples. Samples (5 ± 0.5 mg) were cooled from 20 to −70 °C and then heated to 120 °C with a heating rate of 3 °C min^{-1}. The flow rate of high-purity nitrogen (99.999%) was 80 mL min^{-1}. The content of FW was calculated according to Eq. (1):

$$\mathrm{M_{FW}} = \frac{\Delta H}{H_f} * 100\% \tag{1}$$

where M_{FW} is the content of FW (%), ΔH is the heat released per unit mass of biomass (J g^{-1}), and H_f is the enthalpy of melting of water (333.6 J g^{-1}).

The BW content was obtained using Eq. (2):

$$\mathrm{M}_{BW} = M_t - M_{FW} \tag{2}$$

where M_{BW} is the BW content (%), and M_t is the total water content of the biomass sample (%).

2.3 Experiment of thermogravimetric-differential calorimetric analysis (TG-DSC) and TG-MS

Thermal kinetics were analyzed using a Thermogravimetric-Differential Calorimetric analyzer (TG-DSC, STA 449 F3 Jupiter, NETZSCH) using high-purity nitrogen (99.999%) as the carrier gas. Samples (10 ± 0.5 mg, dry basis) with different water contents were evenly spread in an alumina crucible. The experiment was carried out from 50 to 800 °C with a heating rate of 20 °C min^{-1} and a gas flow rate of 40 mL min^{-1}. DTG curves were obtained by the derivative of the TG curves using the Savitzky-Golay smoothing method. A blank was performed using an empty crucible under the same conditions before the experiment, and the baseline was subtracted.

A quadrupole mass spectrometer (MS, GAM 200) connected to a TG analyzer was used for the online detection of pyrolysis volatiles. The temperature of the connecting tubes was set to 250 ℃ to prevent the condensation of volatiles. The MS ionization energy and range were 70 eV

and 10–500 amu. Selected released gases were recorded at m/z values of 18 for H_2O and 43 for CH_3COOH.

2.4 Kinetics analysis

The activation energy E values (kJ mol^{-1}) were calculated with the Coats-Redfern integral method (Eq. 1), as described in a previous study (Tao et al. 2020a, 2021):

$$\ln\left[\frac{-\ln(1-\alpha)}{T^2}\right] = \ln\frac{AR}{\beta E} - \frac{E}{RT} \tag{3}$$

where α is the conversion rate, R is the g universal gas constant [8.314 J $(mol\ K)^{-1}$], T is the reaction temperature (K), A is a pre-exponential factor (min^{-1}), and β is the heating rate (K min^{-1}). The activation energy E was calculated from the slope of $\ln[(-\ln(1-\alpha))/T^2]$ vs. $1/RT$.

2.5 In situ drift FTIR analysis

In situ drift FTIR (INVENIO, BRUKER, Germany) was used for the online characterization of functional groups during the pyrolysis of raw samples with a series of water contents using high-purity nitrogen as the carrier gas at a flow rate of 40 mL min^{-1}. The samples were mixed with KBr in a ratio of 1:10 (w:w). Measurements were conducted in the wavenumber range of 650–4000 cm^{-1} with a resolution of 4 cm^{-1}. Before pyrolysis, high-purity nitrogen was used to purge the reaction cell for 30 min to remove residual air. During pyrolysis, drift FTIR spectra were collected at pyrolysis temperatures of 300 ℃, 400 ℃, 450 ℃, 500 ℃, 550 ℃, and 600 ℃.

2D-FTIR-COS maps were computed using the discrete Hilbert transform algorithm introduced by Noda (2012). In this approach, each dynamic spectrum y_e (ν, t) was subjected to Fourier transform with respect to the perturbation variable t to obtain its complex form Y_e (ν, ω). The complex cross-correlation functions between different wavenumbers were then calculated.

$$\Phi(\nu_1, \nu_2) + i\Psi(\nu_1, \nu_2) = \frac{1}{2\pi(T_{\max} - T_{\min})} \int_{-\infty}^{\infty} Ye(\nu_1, \omega)\, Ye*(\nu_2, \omega)\mathrm{d}\omega \tag{4}$$

where ν_1 and ν_2 represent independent infrared wavenumbers (cm^{-1}), corresponding to the abscissa and ordinate of the two-dimensional correlation spectra, respectively; $\Phi(\nu_1, \nu_2)$ represents the synchronous spectrum; $\Psi(\nu_1, \nu_2)$ represents the asynchronous spectrum; $\frac{1}{(T_{max}-T_{min})}$ is a normalization factor, whose purpose is to normalize the results to the temperature range [$T_{\min}$, $T_{\max}$]; ω is the angular frequency (rad s^{-1}) after Fourier transform; $Ye(\nu_1, \omega)$ and $Ye*(\nu_2, \omega)$ are the complex form and its complex conjugate after Fourier transform, which are used to calculate the cross-correlation.

2D-FTIR-COS extended the one-dimensional spectral variations into a two-dimensional domain, which generated synchronous and asynchronous correlation maps. The features of these synchronous and asynchronous maps were interpreted according to Noda's rules (Noda 2012). Briefly, automatic peaks in the synchronous spectra indicate the changes to the peaks at the corresponding position, and the cross-peaks represent synchronous changes to spectral signals at different wavenumbers. A given peak or region exhibiting the same sign in both the synchronous and asynchronous spectra suggests that the change in absorption intensity of this variable mainly occurs before that of another variable during the perturbation. Conversely, if the signs are opposite, the sequence is reversed. Moreover, if the synchronous cross-peak at that position is close to zero, the sequential order of the absorption changes cannot be determined.

3 Results and discussion

3.1 DSC analysis of CL, LG, and RS with different water contents

As shown in Fig. 1, one exothermic and two endothermic peaks appeared in the DSC thermograms of CL, LG, and RS samples. Exothermic peaks appeared during the cooling processes (Fig. 1a, c, and e) due to the phase transition from liquid water to ice. The two endothermic peaks during the heating process were attributed to the melting of ice and the evaporation of water, respectively. After water completely evaporated, the DSC curve became a straight line, indicating no thermal effects for CL, LG, and RS samples with different water contents.

Upon decreasing the temperature, an exothermic peak appeared near −14 ℃ for the CL samples, which revealed the existence of freezable FW. When the water content decreased to 29.92%, the intensity of the freezable FW peak decreased sharply and disappeared completely when the water content was 19.97%. No exothermic peak appeared in the DSC curves for CL samples with water contents of 19.97% and 10.05%, because the freezable FW mainly existed in capillaries and interparticle spaces (Hill et al. 2024). During heating, two endothermic peaks appeared in the range of −60 to 120 ℃. The smaller peak near 0 ℃ was attributed to the melting of ice produced by freezable FW during cooling, and the larger endothermic peak was due to the evaporation of non-freezable and thawed water. Neither the cooling nor heating curves of CL samples with water contents lower than 19.97% showed exothermic peak (Fig. 1a and b). However, one water evaporation peak was observed during the heating process due to the thermal release of BW from CL samples. BW commonly refers to water that is hydrogen

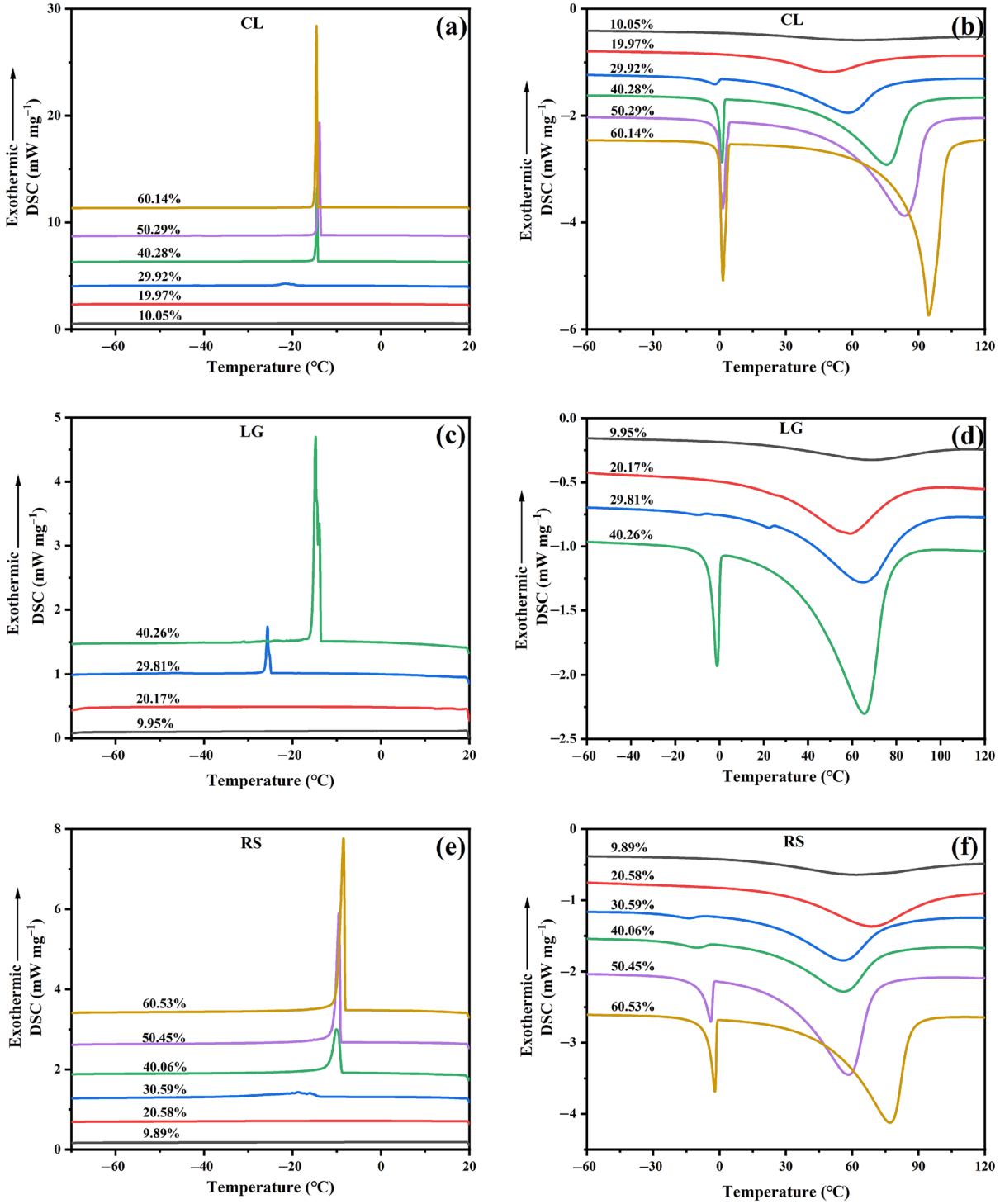

Fig. 1 DSC thermograms during the cooling process of CL (**a**), LG (**c**), and RS (**e**), and during the heating process of CL (**b**), LG (**d**), and RS (**f**) with different water contents

bonded to proteins, lignin, and polysaccharides and is commonly found within the cells and cell walls of lignocellulosic biomass (Khan et al. 2018).

LG and RS samples with different water contents were analyzed using DSC to determine their FW and BW contents. The water content of LG samples was in the range

of 9.95–40.26%. When the water content was higher than 40.26%, flowing water was clearly visible in the LG samples. The freezable FW peak shifted to a lower temperature upon decreasing the water content (Fig. 1c). When the water content decreased from 40.26% to 29.81%, the FW peak shifted from −15 to −25 °C, possibly due to the presence of FW in LG. For RS samples, when the water content was increased from 30.59% to 60.53%, the intensity of the FW peak increased near-monotonically. When the water content was lower than 30.59%, no exothermic peaks were observed during the freezing process, which was also observed in CL and LG samples.

The exothermic peak area was integrated to calculate the FW content. As shown in Figure S1, the FW content in CL was greater than that in LG with a similar initial water content, indicating that CL was better at absorbing and retaining water than LG. During water adsorption, the main adsorption sites were mainly hydrophilic groups, such as hydroxy and carboxyl groups. Water molecules tended to break the hydrogen bonds between polymer chains and then form new hydrogen bonds between the polymer chains. This type of water was BW. The fiber saturation of CL was around 20%, which was lower than that of RS (24%) and LG (28%). This difference was attributed to the ordered crystalline structure of CL. Upon increasing the water content, water molecules began to form hydrogen bonds between themselves, indicating the existence of FW.

3.2 TG and DTG analysis of CL, LG, and RS with different water contents

3.2.1 TG and DTG analysis of CL and LG

Figure S2 shows the TGA and DTG profiles of the pyrolysis of CL and LG from 50 to 800 °C at a heating rate of 20 ℃ min^{-1}. The water content was calculated from the TGA curves using the mass loss below 150 ℃. The water contents of CL and LG determined by oven and TGA were obviously different (Figure S3). The water content measured by the oven was significantly higher than that calculated from the TGA data, indicating that the water was not fully released below 150 ℃. Unreleased water may have participated in pyrolysis reactions. In the DTG curves, the first peak below 150 ℃ belonged to the mass loss of water (Tp-w), and the second peak was the main pyrolysis peak of CL (Tp-CL, Figure S2b) and LG (Tp-LG, Figure S2d). Compared with the broad main pyrolysis stage of LG, CL showed a narrower main pyrolysis temperature range of 300–400 ℃ because of the different molecular structures of CL and LG. Unlike the ordered hexagonal rings of CL, LG contains amorphous aromatic polymers with a higher thermal stability (Tai et al. 2023).

To clarify how the different types of water influenced on Tp-w, Pearson correlation was used to generate the relationship between the DTG peak center temperature of CL (Tp-CL) and LG (Tp-LG) and the absolute dry mass loss of CL (CL%) and LG (LG%) (Figure S4). The value of Tp-w moved to a higher temperature upon increasing the water (W) and FW contents. No linear correlation was found between W and Tp-CL, but a negative linear correlation ($p < 0.05$) was established between Tp-LG vs. W and Tp-LG vs. BW. The differential influence of water on Tp-CL and Tp-LG was due to the bonding energy and hydrogen bonding modes in CL and LG.

3.2.2 TG and DTG analysis of RS with different water contents

The TGA and DTG curves of RS samples with different water contents are shown in Fig. 2. The DTG curves of RS with different water contents consisted of four main peaks, where the first peak in the range of 90–117 °C was attributed to the release of water during heating. The

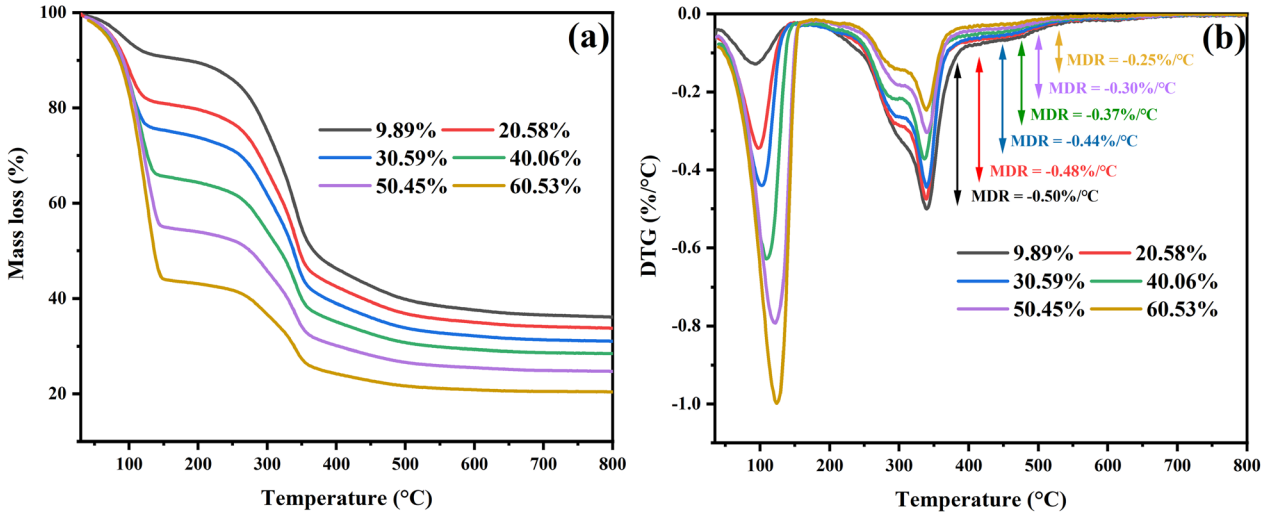

Fig. 2 TGA (**a**) and DTG (**b**) curves of RS samples with different water contents

shoulder peak near 307–313 ℃ and the sharp peak centered at 341 ℃ were attributed to the thermal decomposition of hemicellulose (HC) and CL, respectively (Tao et al. 2020a). The wider peaks at 427–450 °C were related to the LG pyrolysis (Nhuchhen and Basu 2014). Similar to the result of CL and LG, the water contents obtained by the oven-drying method were much higher than those calculated from the TGA data (Figure S5), demonstrating that unreleased water participated in pyrolysis reactions.

The correlation between W, FW, BW, Tp-w, Tp-HC, Tp-CL, and Tp-LG is shown in Figure S6. Positive linear correlations were found between Tp-w and W, FW, and BW, implying that both FW and BW increased the amount of energy required to fully evaporate water. No linear correlation was found between Tp-CL and W, consistent with the CL samples (Figure S4a). A significant negative linear correlation was found between BW and Tp-HC ($r = -0.85$, $p < 0.05$). Similar to the LG samples, a negative correlation was found between W and Tp-LG and between BW and Tp-LG, indicating that BW in RS promoted the thermal decomposition of HC and LG.

3.2.3 *Effect of water on the maximum decomposition rate*

The correlation between water and the maximum decomposition rate (MDR) of CL, LG, and RS is shown in Fig. 3. MDR is the instantaneous reaction rate and reflects the intensity of pyrolysis reactions. Significant negative correlations were observed between W and MDR for CL, LG, and RS, indicating that upon increasing the water content, the instantaneous pyrolysis reaction rates greatly decreased. This was primarily attributed to the endothermic vaporization of water, which decreased the overall

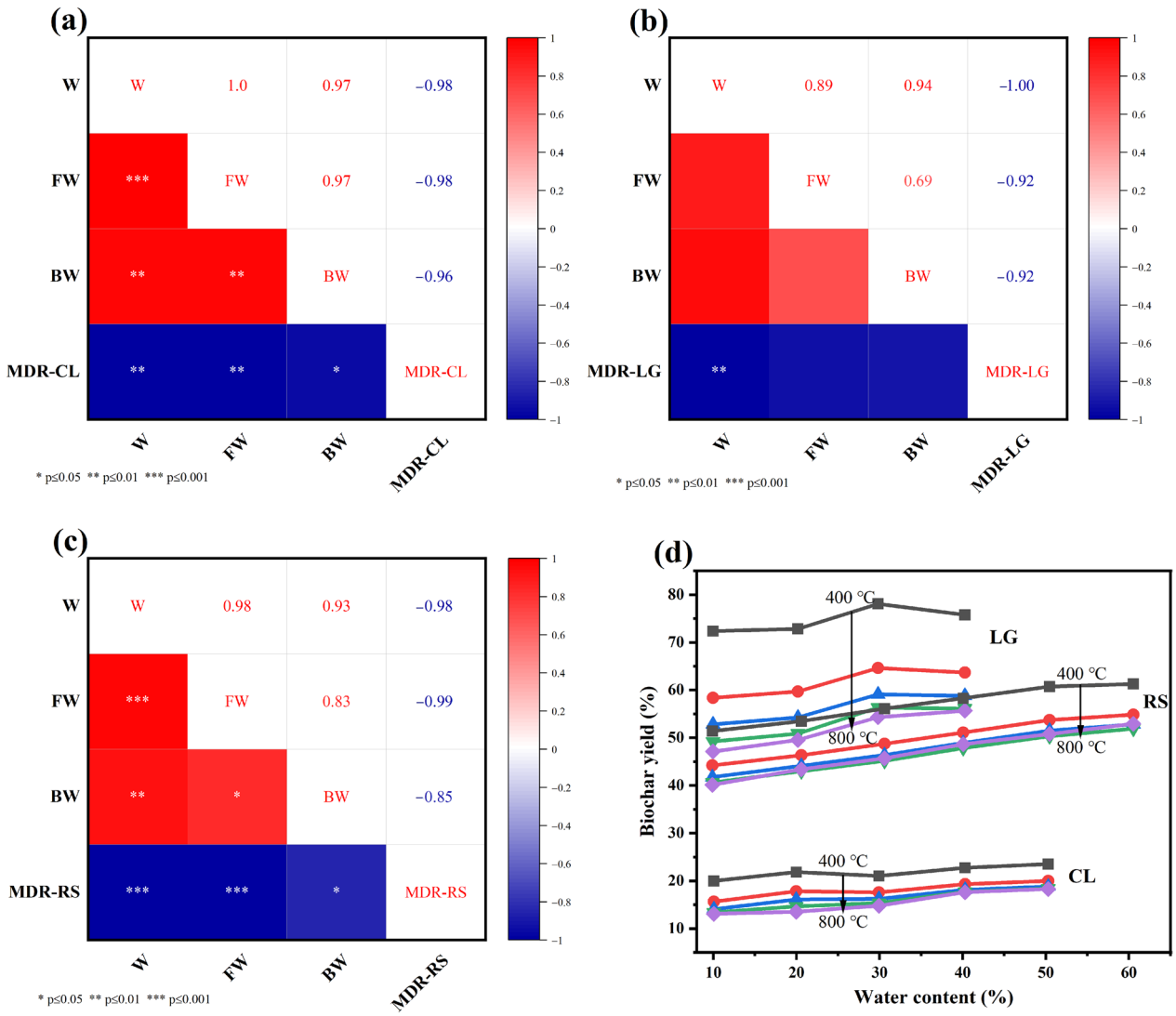

Fig. 3 Correlation between water content (W), free water (FW) content, bound water (BW), and MDR of CL (**a**), LG (**b**), and RS (**c**); the relationship between the water (W) content and biochar yield (**d**)

heating rate and actual reaction temperature, and the slower reaction rate promoted biochar formation.

To further investigate the effect of water on biochar yield, the relationship between water content and biochar yield was plotted (Fig. 3d). As the water content increased from 10% to 60%, the biochar yield was correspondingly increased for all samples, with LG derived biochar showing the highest yield of 78%. According to the linear fit in Figure S7, the slopes of biochar yield vs. water content were 0.30, 0.25, and 0.14 for LG, RS, and CL, respectively. This showed that water promoted thermal decomposition in the order of CL > RS > LG. That is, water tended to react with CL rather than LG during pyrolysis, as LG has a stable aromatic structure that does not significantly interact with water during pyrolysis, allowing it to retain its carbonaceous skeleton (Chen et al. 2023). In contrast, CL is an ordered polysaccharide with a lower thermal stability, so it readily underwent rapid cracking when it contacted water.

Although high water content resulted in a high biochar yield, it also increased the energy consumption and costs. The endothermic peaks of water from TG-DSC were used to calculate the additional energy consumed during pyrolysis. As shown in Figures S8 and S9, the energy consumption of CL, LG, and RS sharply increased upon increasing the water content. Considering the energy consumption and biochar yield, the water content of biomass pyrolysis should be controlled at around 30%.

3.3 Kinetics analysis of CL, LG, and RS with different water contents

3.3.1 Pyrolysis kinetics of CL and LG

The pyrolysis kinetics during the main pyrolysis stage of CL and LG were investigated using the Coats-Redfern integration method. The fitting equations and activation energies are shown in Table 1. The coefficients of determination (R^2) of the fitting lines were greater than 0.97, indicating that the calculated activation energies for CL and LG samples were feasible. The correlation between water and activation energy E for CL and LG is shown in Figure S10. A significant positive linear correlation was found between E and W, and between E and FW in CL samples, indicating that FW affected E for CL samples. However, as presented in Figure S10b, the E values of LG linearly decreased upon increasing the BW content. CL is a polysaccharide composed of glucose units linearly linked by β−1,4-glycosidic bonds (Chen et al. 2022b), which form highly ordered crystalline microfibrils stabilized by extensive intra- and intermolecular hydrogen bonds (Jarvis 2023). Water formed additional hydrogen bonds with the hydroxy groups of CL, which enhanced its overall structural stability. As a result, increasing the water content increased the pyrolytic activation energy of CL. In contrast, LG is an amorphous, highly cross-linked aromatic macromolecule containing numerous polar functional groups, such as phenolic hydroxy groups. The integrity of its internal structure partially relies on a hydrogen-bonded network between these polar groups, which is far less ordered than that of CL. Bound water can establish hydrogen bonds with the hydroxy and ether groups of LG, inserting and disrupting the original intermolecular hydrogen-bond network and exhibiting a plasticizing effect (Henrik-Klemens et al. 2025). This water-induced disruption of hydrogen bonding may have increased the mobility of LG chains and reduced their thermal stability, causing the activation energy of LG samples to decrease linearly upon increasing the BW content.

Table 1 Calculated activation energy E of CL and LG

Sample	Water content (%)	Equation	R_{adj}^2	E (kJ mol^{-1})	Error
CL	10.05	$y=-33913x+51.98$	0.9899	339.13	5.21
	19.97	$y=-33858x+51.87$	0.9893	338.58	5.35
	29.92	$y=-33300x+50.65$	0.9943	333.00	3.87
	40.28	$y=-31883x+47.73$	0.9776	318.83	7.45
	50.29	$y=-35315x+54.56$	0.9954	353.15	3.75
LG	9.95	$y=-58586x-2.52$	0.9880	58.59	0.46
	20.17	$y=-57724x-2.64$	0.9858	57.72	0.50
	29.81	$y=-57121x-2.73$	0.9850	57.12	0.51
	40.26	$y=-55834x-2.93$	0.9856	55.83	0.49

3.3.2 Pyrolysis kinetics of RS

According to the DTG analysis of RS in Sect. 3.2.2, the main pyrolysis step was the thermal decomposition of HC, CL, and LG. To calculate activation energy E, the overall pyrolysis process was divided into the pyrolysis of HC, CL, and LG, respectively (Figures S11–S13 and Table 2). The fitted correlation coefficients (R_{adj}^2) were all greater than 0.97, indicating that the Coats-Redfern integral method was suitable for the kinetic analysis of RS with different water contents. The activation energy E of CL (E-CL) was higher than those of HC and LG, consistent with our previous results (Tao et al. 2020a, 2021). Additionally, the value of E-CL in RS was lower than that of the pure CL biopolymer (Table 1), possibly because alkali and alkaline metals in RS catalyzed the pyrolysis of CL (Wang et al. 2022). However, the value of E-LG in RS was higher than that of the LG biopolymer (Table 1) because the residual char of CL and HC further decomposed in the temperature range used to calculate E-LG.

According to Table 2, water exerted distinct effects on the pyrolysis reactions of HC, CL, and LG. Water evaporation absorbed a large amount of heat and delayed

Table 2 Kinetic fitting results for each interval during the main pyrolysis stage of rice straw

Water content (%)	*E*-HC (kJ mol^{-1})	R_{adj}^2	*E*-CL (kJ mol^{-1})	R_{adj}^2	*E*-LG (kJ mol^{-1})	R_{adj}^2
9.89	95.608 ± 0.61	0.9975	157.960 ± 4.61	0.9799	77.063 ± 0.94	0.9871
20.58	94.058 ± 0.36	0.9993	186.209 ± 5.35	0.9837	77.084 ± 0.90	0.9880
30.59	93.099 ± 0.32	0.9994	282.582 ± 8.53	0.9812	79.418 ± 0.95	0.9877
40.06	92.715 ± 0.25	0.9997	285.810 ± 8.04	0.9836	80.631 ± 1.69	0.9853
50.45	92.952 ± 0.37	0.9992	284.783 ± 8.64	0.9819	78.633 ± 0.91	0.9884
60.53	90.257 ± 0.23	0.9997	277.723 ± 8.67	0.9799	79.267 ± 0.98	0.9869

the apparent pyrolysis onset temperature of the samples (Sharma et al. 2015). The hydrogen bonds formed between water and polymers may have also changed the pyrolysis mechanism. The relationship between water and the activation energy *E* of HC, CL, and LG in RS is shown in Figure S14 to further clarify the mechanism by which water influenced the pyrolysis of HC, CL, and LG. *E*-HC showed significant negative correlations with water content, FW, and BW, indicating that a higher water content decreased the energy required for HC pyrolysis. In contrast, *E*-CL showed a significant positive correlation with total water and BW, consistent with Figure S10a. *E*-LG remained largely unaffected by variations in the water content.

The marked decrease in *E*-HC upon increasing the water content was attributed to its highly amorphous structure and abundant of hydrophilic functional groups, such as acetyl and hydroxy groups, which readily interacted with water to form extensive hydrogen-bond networks. When water penetrated the HC matrix, it disrupted intermolecular hydrogen bonds, reduced the degree of polymerization, and enhanced chain mobility (Elf et al. 2023). Water may have also participated in hydrolysis reactions or facilitated heat transfer during pyrolysis, thereby promoting thermal cleavage of HC at lower temperatures (Tu et al. 2022), consistent with the results in Figure S6.

Water, especially BW, could tightly associate with CL via hydrogen bonding and thus required much higher temperatures and energy for thermal release. The BW attached to CL chains served as a thermal buffer during pyrolysis, which enhanced its thermal stability (Paajanen et al. 2019). Bound water (hydrogen-bonded water adsorbed within cellulose) could form additional hydrogen bonds with cellulose's hydroxyls groups. It intercalated between chains and partially disrupted interchain

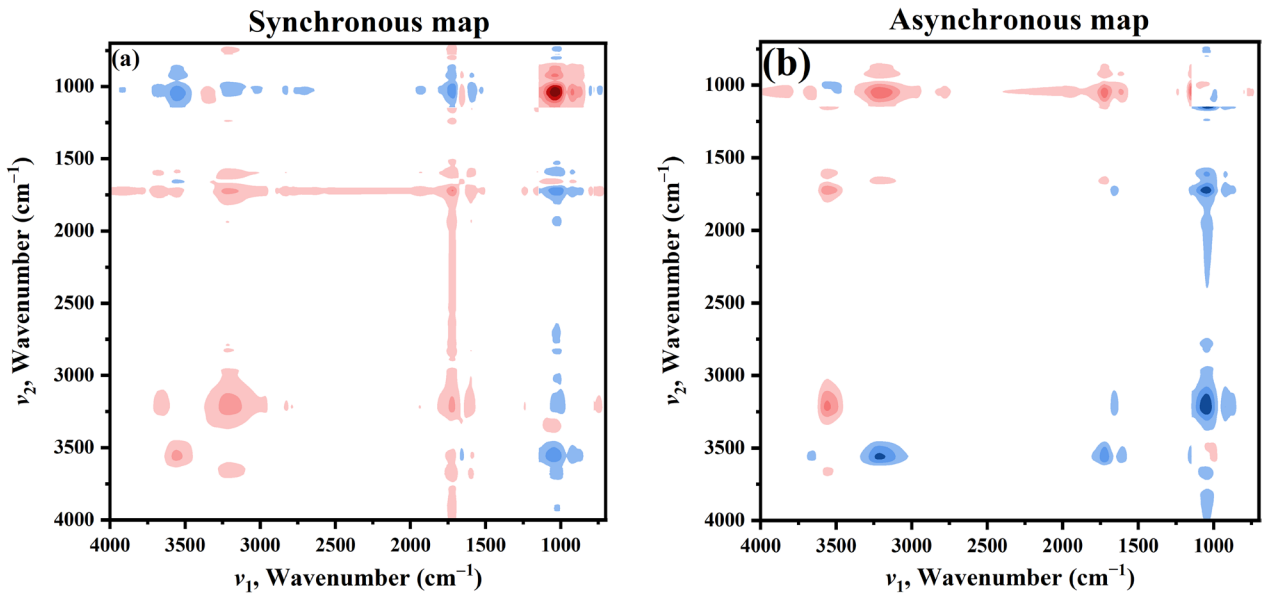

Fig. 4 2D-FTIR-COS spectra for RS-derived biochar (pyrolysis temperature at 500 ℃) with the water content of raw samples as the disturbance: synchronous spectra (**a**) and asynchronous spectra (**b**). Red and blue areas represent positive and negative correlations, respectively. The darker color indicates the higher absolute correlation coefficient. In the synchronous and asynchronous maps, the cross-peaks in the upper-left were counted and analyzed

hydrogen bonding, while concurrently bridging cellulose and water to reinforce the hydrogen-bond network. The BW connected to CL chains further increased the energy required for pyrolysis.

LG showed the opposite behavior, in which *E*-LG remained stable under different water contents. Although water could form new hydrogen bonds with hydroxy and ether groups within LG, it could also preferentially interact with HC and CL (Zitting et al. 2024). LG did not significantly change with water content.

3.4 Pyrolysis biochar structure determination from 2D-FTIR-COS

The different functional groups in this complex pyrolysis system might have overlapping vibrational peaks in their one-dimensional drift FTIR spectra (Figure S15 and Table S2), such as the FW O–H and BW O–H, and the carboxyl C=O and carbonyl C=O. These overlapping peaks might have different responses to the water content. Therefore, two-dimensional FTIR correlation spectroscopy (2D-FTIR-COS) was used to better understand the subtle but important differences, correlations, and sequential changes in functional groups in response to the water content. As shown in Figs. 4 and S16, the red and blue colors for auto/cross-peaks represent the positive and negative correlations, respectively. ν_1 and ν_2 are a pair of independent 2D-FTIR-COS wavenumbers that correspond to the *x*-axis and *y*-axis in the synchronous and asynchronous maps, respectively (Noda 2012). The 2D-FTIR-COS results on the sign of each cross-peak in synchronous and asynchronous maps are listed in Table S3.

In the synchronous map, five positive auto-peaks were present near 3600, 3150, 1730, 1630, and 1050 cm^{-1} (Figs. 4 and S16). These synchronous auto-peaks were associated with the specific species of O–H, aromatic C–H, carboxyl C=O, aromatic C=C, and carbohydrates C–O–C, respectively (Bodîrlau and Teaca 2009; Martín et al. 2005). This result suggests that the contents of these groups were relatively sensitive to the water content changes. Several positive cross-peaks, such as those at ν_1/ν_2 values of 3600/3150, 1730/1630, 1630/900, 1460/(1080, 1070, 900), and 1070/900 cm^{-1}, revealed that these functional groups changed in the same direction or trend upon increasing the water content. Additionally, the synchronous map also exhibited a weak off-diagonal peaks with negative signals at (3580/3200) cm^{-1} with the pyrolysis temperature lower than 400 ℃ (Figure S16c). This indicated that the –OH groups of FW and BW or polymers exhibited some degree of mutual inhibition or competition upon increasing the water content during pyrolysis process. Taking the reaction of water and cellulose as an example, the –OH groups of cellulose can interact with each other to form hydrogen bonds. However, BW can break the original hydrogen bonds in cellulose and generate a stronger hydrogen bond network, thus improving the stability and activation energy of cellulose (Etale et al. 2023).

The asynchronous map revealed sequential changes in different functional groups in response to the water content. According to Noda's rule, if the peak/region signals in the synchronous/asynchronous maps are identical, the overall change in spectral intensity at ν_1 predominantly occurs before ν_2, while the reaction order is reversed when the signs are different (Noda 2004). As shown in Table S3, a common sequential water response of functional groups was found to be: hydroxyl → carboxyl C=O → aliphatic C–H → carbohydrates C–O–C → aromatic rings. This order is consistent with the reaction activity of these groups and the enhancement in aromaticity during pyrolysis. The cross-peak at (3580/3200) cm^{-1} indicated the release of free and bound water. Within the temperature range of 400–500 ℃ (Figs. 4, S13c and S13d), the delayed variations in BW became more obvious, a trend that became amplified at higher temperatures. Hydroxyl and aliphatic C–H are more reactive and prone to cleavage. The positive value of (1730/1630) cm^{-1} indicated that water promoted the reaction from carboxyl C=O to carbonyl C=O groups. For example, water could hydrolyze the carboxyl C=O groups to promote the removal of the acetyl group during the pyrolysis of hemicellulose (Li et al. 2014; Abu Tayeh et al. 2016).

3.5 Online TG-MS detection of the release of H_2O and CH_3COOH

The release of H_2O and CH_3COOH during pyrolysis was detected online by TG-MS. As shown in Fig. 5, upon increasing the water content, more H_2O and CH_3COOH were released. The peaks of released H_2O were divided into two temperature ranges of 90–150 ℃ (peak-1) and 300–400 ℃ (peak-2). Upon increasing the water content, peak-1 of H_2O shifted to higher temperatures ($r=0.79$, $p<0.05$), and peak-2 of H_2O shifted to lower temperatures ($r=-0.70$, $p<0.05$). The linear fit of the central peak temperature and water content verified that a higher water content promoted the release of peak-1 at higher temperatures and the release of peak-2 at lower temperatures (Figure S17a), which aligns with the DSC results. This phenomenon may stem from the formation of hydrogen bonds and analogous structures between BW and the RS structure during the initial pyrolysis stage, thereby requiring a higher temperature for water release. Upon increasing the pyrolysis temperature, a higher water content facilitated the thermal desorption of RS, which decreased the release temperature of H_2O.

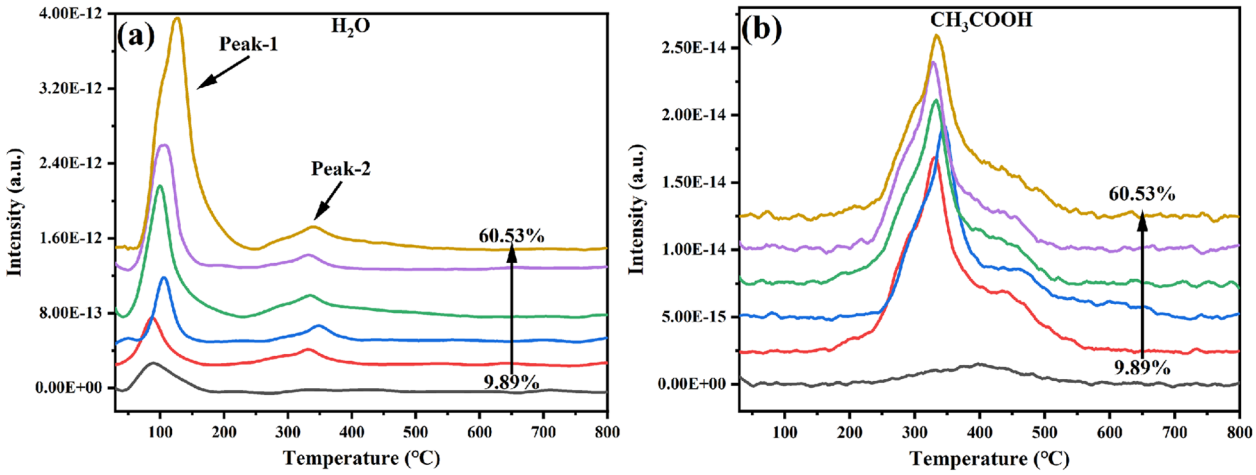

Fig. 5 TG-MS online detection of H_2O ($m/z = 18$) and CH_3COOH ($m/z = 43$) during pyrolysis

Additionally, the relationship between peak area and water content was fitted (Figure S17b). For peak-1 and peak-2, the *r* values of their linear fits were 0.88 and 0.89. The FW content increased linearly with increasing the water content, while BW participated in decomposition reactions and promoted the thermal release of water during pyrolysis.

CH_3COOH was the main pyrolysis gas evolved from HC (Tao et al. 2020b). As shown in Fig. 5b, the release peak of CH_3COOH was in the range of 250–400 ℃. Upon increasing the water content, the peak center temperature of CH_3COOH also underwent a linear shift to a lower temperature ($r = -0.84$, $p < 0.05$, Figure S18a). The relationship between the integral area of the CH_3COOH peak and water content was analyzed by linear fitting. As shown in Figure S18b, the released amount of CH_3COOH linearly increased with increasing the water content ($r = 0.94$, $p < 0.05$). The above analysis revealed

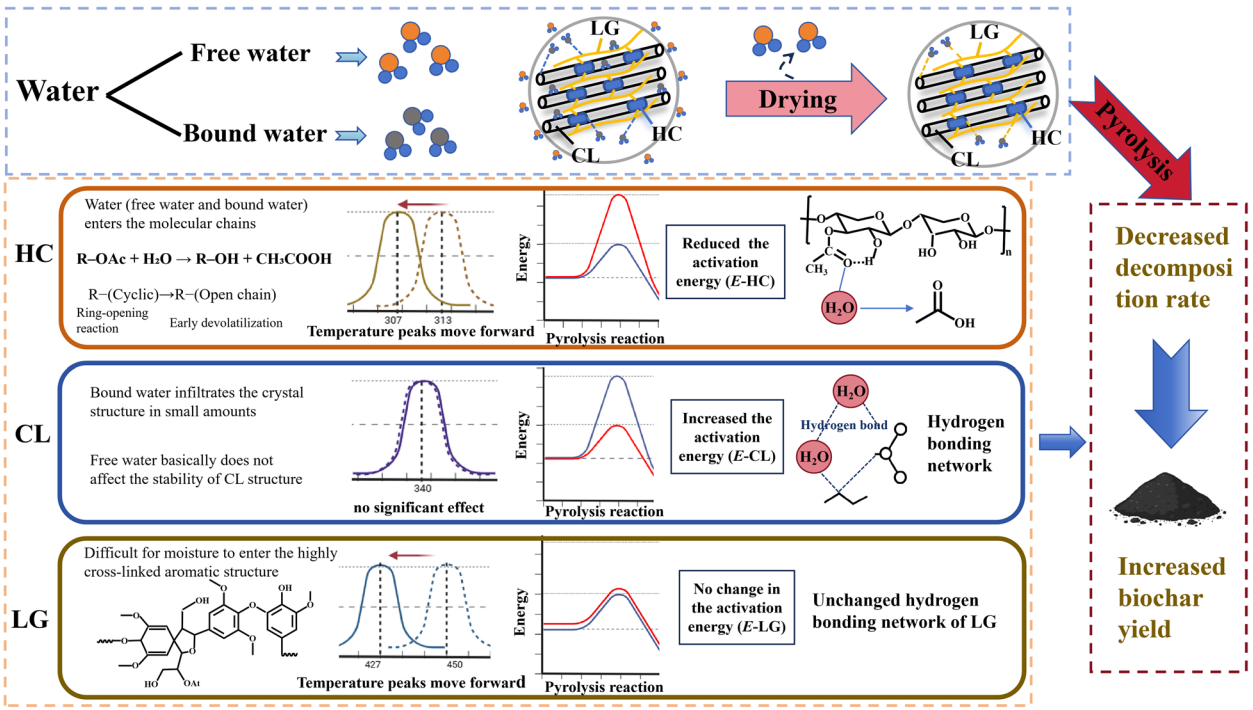

Fig. 6 Mechanism by which water influenced lignocellulose pyrolysis

that water promoted the deacetylation of HC, consistent with the 2D-FTIR-COS results.

3.6 Influence mechanism of water on lignocellulose pyrolysis

Based on the above results and discussion, a schematic diagram was used to illustrate the influence of water on the pyrolysis mechanism of RS (Fig. 6). During the initial stage of pyrolysis, the evaporation of water absorbed a large amount of heat and decreased the apparent pyrolysis onset temperature of the sample (Sharma et al. 2015). In contrast, BW was tightly associated with CL and HC via hydrogen bonding and required much higher temperatures and energy for thermal release, causing the maximum mass-loss peak to shift to much higher temperatures. The combined effects of both FW and BW significantly decreased the intensity of the pyrolysis reaction, inhibited the release and diffusion of volatiles, and slowed down the thermal decomposition of biomass components. Therefore, more organic matter was retained in the solid phase, and thus increased biochar yield.

HC contains highly branched O-acetyl groups in its amorphous molecular structure, and water tended to form hydrogen bonds with O-acetyl groups to promote its hydrolysis (Wang et al. 2021), which decreased the activation energy. Combined with the 2D-FTIR-COS and TG-MS results, BW formed hydrogen bonds with hydroxyl and carbonyl groups and disrupted the intrinsic hydrogen bond network of HC, which facilitated chain scission during hydrolysis and deacetylation. This promoted ring-opening and decarboxylation, enabled the cleavage of –OH and C–O–C groups, and decreased the activation energy of pyrolysis.

In contrast, water increased the activation energy of CL, whose functional groups mainly included hydroxyl groups and β−1,4-glycosidic bonds that could form hydrogen bonds with water. Additionally, crystallized CL had strong intra- and inter-chain hydrogen bonds that increased the thermal stability of CL. BW intercalates between cellulose chains via hydrogen bonds, further increasing the structural stability of CL. The formed hydrogen bond network increased the activation energy of thermal decomposition (Etale et al. 2023).

Due to its abundant aromatic ethers and C=C bonds, LG had a higher thermal stability than both HC and CL. When the water content increased from 10% to 40%, the maximum decomposition peak temperature shifted from 450 to 427 °C, indicating an earlier onset of decomposition for LG. 2D-FTIR-COS and Py-GC results demonstrated that water markedly accelerated the decomposition of O-alkyl groups, as well as the release of CH_4. However, water had a limited ability to alter the stable aromatic framework of LG, so the activation energy of LG remained unchanged.

4 Conclusion

This study investigated how the type and behavior of water affected the pyrolysis of biomass. The results showed that as the water content increased, the maximum mass loss rates of CL, LG, and RS all greatly decreased, which indicated that water decreased the intensity of the pyrolysis reaction. The increase in the biochar yield of CL, LG, and RS upon increasing the water content further confirmed this hypothesis. Considering the energy consumption with the biochar yield, the water content in biomass should be controlled at around 30% during pyrolysis. Water promoted the thermal decomposition of HC, and the release of acetic acid shifted to low temperatures at high water contents. However, the hydrogen bond network between BW and CL increased the overall structural stability of CL. The sequential water response of functional groups followed the order: hydroxyl → carboxyl C=O → aliphatic C–H → carbohydrate C–O–C → aromatic rings. The rapid weakening of the absorption peaks of –OH and C=O and the intensified absorption peaks of aromatic C=C bonds in 2D-FTIR-COS spectra suggest that water promoted the formation of condensed aromatic carbon structures. These findings provide a theoretical basis for optimizing biochar production and physicochemical properties by regulating the water content of feedstocks. These findings also provide a basis for regulating the water content of lignocellulosic feedstocks to tailor the pyrolysis product distribution and promote the utilization of biomass resources.

Only RS was selected to represent lignocellulosic biomass in this study, and the interactions between water and ash were neglected due to the low ash content in the selected biomass. In future work, a wider selection of biomass with higher ash contents will be used to reduce the limitations of this work and further investigate the effect of initial water content on pyrolysis reactions across different biomass species.

Supplementary Information

The online version contains supplementary material available at https://doi.org/10.1007/s42773-026-00629-5.

Supplementary material 1.

Author contributions

Wenmei Tao: Investigation, Writing – original draft. Linjian Gao: Data curation, Writing – original draft. Mengzi Li: Writing – review & editing. Yunzhu Wang: Writing – review & editing. Lin Shi: Writing – review & editing. Chengcheng Xu: Writing – review & editing. Xinyuan Lu: Writing – review & editing. Bo Pan: Supervision. All authors read and approved the final manuscript.

Funding
This research was supported by National Natural Scientific Foundation of China (42207286 and 42567031), Yunnan Fundamental Research Projects (202401AT070385, 202201BE070001-041), and Yunnan Key Laboratory of Efficient Utilization and Intelligent Control of Agricultural Water Resources.

Data availability
The datasets used or analyzed during the current study are available from the corresponding author upon reasonable request.

Declarations

Competing interests
Bo Pan is an EBM of the journal Biochar, and he was not involved in the peer-review or handling of the manuscript. The authors declare that they have no known competing financial interests or personal relationships that could have appeared to influence the work reported in this paper.

Author details
[1]Faculty of Modern Agricultural Engineering, Kunming University of Science and Technology, Kunming 650500, Yunnan, China. [2]Yunnan Provincial Key Laboratory of Soil Carbon Sequestration and Pollution Control, Faculty of Environmental Science & Engineering, Kunming University of Science and Technology, Kunming 650500, China. [3]Research Center for Analysis and Measurement, Kunming University of Science and Technology, Kunming 650500, China. [4]College of Resources and Environment, Linyi University, Linyi 276005, China.

Received: 6 January 2026 Revised: 14 April 2026 Accepted: 26 April 2026
Published online: 22 June 2026

References

Abu Tayeh H, Levy-Shalev O, Azaizeh H, Dosoretz C (2016) Subcritical hydrothermal pretreatment of olive mill solid waste for biofuel production. Bioresource Technol 199:164–172
Akhtar J, Amin NS (2012) A review on operating parameters for optimum liquid oil yield in biomass pyrolysis. Renew Sust Energy Rev 16:5101–5109
Bikbulatova S, Tahmasebi A, Zhang Z, Rish S, Yu J (2018) Understanding water retention behavior and mechanism in bio-char. Fuel Process Technol 169:101–111
Bodîrlau R, Teaca C (2009) Fourier transform infrared specgtroscopy and thermal analysis of lignocellulose fillers treated with organic anhygrides. Rom J Phys 54:93–104
Carpenter D, Westover TL, Czernik S, Jablonski W (2014) Biomass feedstocks for renewable fuel production: a review of the impacts of feedstock and pretreatment on the yield and product distribution of fast pyrolysis bio-oils and vapors. Green Chem 16:384–406
Chen D, Cen K, Zhuang X, Gan Z, Zhou J, Zhang Y, Zhang H (2022a) Insight into biomass pyrolysis mechanism based on cellulose, hemicellulose, and lignin: evolution of volatiles and kinetics, elucidation of reaction pathways, and characterization of gas, biochar and bio-oil. Combust Flame 242:112142
Chen P, Wohlert J, Berglund L, Furó I (2022b) Water as an intrinsic structural element in cellulose fibril aggregates. J Phys Chem Lett 13:5424–5430
Chen C, Sun K, Huang C, Yang M, Fan M, Wang A, Zhang G, Li B, Jiang J, Xu W, Liu J (2023) Investigation on the mechanism of structural reconstruction of biochars derived from lignin and cellulose during graphitization under high temperature. Biochar 5:51
Elf P, Ozeren H, Larsson P, Larsson A, Wagberg L, Nilsson R, Chaiyupatham P, Hedenqvist M, Nilsson F (2023) Molecular dynamics simulations of cellulose and dialcohol cellulose under dry and moist conditions. Biomacromol 24:2706–2720
Etale A, Onyianta AJ, Turner SR, Eichhorn SJ (2023) Cellulose: a review of water interactions, applications in composites, and water treatment. Chem Rev 123:2016–2048
Gao A, Wang Y, Lin G, Li B, Hu X, Huang Y, Zhang S, Zhang H (2022) Volatile-char interactions during biomass pyrolysis: reactor design toward product control. Renew Energy 185:1–7
Henrik-Klemens A, Edlund U, Westman G, Larsson A (2025) Dynamic mechanical analysis of plasticized and esterified native, residual, and technical lignins: compatibility and glass transition. ACS Sustain Chem Eng 13:648–1656
Hill C, Altgen M, Penttila P, Rautkari L (2024) Review: interaction of water vapour with wood and other hygro-responsive materials. J Mater Sci 59:7595–7635
Jarvis MC (2023) Hydrogen bonding and other non-covalent interactions at the surfaces of cellulose microfibrils. Cellulose 30:667–687
Jerzak W, Reinmoeller M, Magdziarz A (2022) Estimation of the heat required for intermediate pyrolysis of biomass. Clean Technol Environ Policy 24:3061–3075
Khan MIH, Joardder MUH, Kumar C, Karim MA (2018) Multiphase porous media modelling: a novel approach to predicting food processing performance. Crit Rev Food Sci Nutr 58:528–546
Li Y, Liu W, Hou Q, Han S, Wang Y, Zhou D (2014) Release of acetic acid and its effect on the dissolution of carbohydrates in the autohydrolysis pretreatment of poplar prior to chemi-thermomechanical pulping. Ind Eng Chem Res 53:8366–8371
Liu H, Zhang Q, Hu H, Li A, Yao H (2014) Influence of residual moisture on deep dewatered sludge pyrolysis. Int J Hydrogen Energy 39:1253–1261
Luo Q, Bai Y, Wei J, Song X, Lv P, Wang J, Su W, Lu G, Yu G (2023) Insights into the oxygen-containing groups transformation during coal char gasification in H_2O/CO_2 atmosphere by using ReaxFF reactive force field. J Energy Inst 109:101293
Martín J, Solla A, Woodward S, Gil L (2005) Fourier transform-infrared spectroscopy as a new method for evaluating host resistance in the Dutch elm disease complex. Tree Physiol 25:1331–1338
Nhuchhen DR, Basu P (2014) Experimental investigation of mildly pressurized torrefaction in air and nitrogen. Energy Fuels 28:3110–3121
Noda I (2004) Advances in two-dimensional correlation spectroscopy. Vib Spectrosc 36:143–165
Noda I (2012) Close-up view on the inner workings of two-dimensional correlation spectroscopy. Vib Spectrosc 60:146–153
Nwaka D, Tahmasebi A, Tian L, Yu J (2016) The effects of pore structure on the behavior of water in lignite coal and activated carbon. J Colloid Interface Sci 477:138–147
Paajanen A, Ceccherini S, Maloney T, Ketoja JA (2019) Chirality and bound water in the hierarchical cellulose structure. Cellulose 26:5877–5892
Pang S, Mujumdar AS (2010) Drying of woody biomass for bioenergy: drying technologies and optimization for an integrated bioenergy plant. Dry Technol 28:690–701
Sharma A, Pareek V, Zhang D (2015) Biomass pyrolysis-a review of modelling, process parameters and catalytic studies. Renew Sust Energy Rev 50:1081–1096
Shinners KJ, Binversie BN, Muck RE, Weimer PJ (2007) Comparison of wet and dry corn stover harvest and storage. Biomass Bioenergy 31:211–221
Sluiter A, Hames B, Ruiz R, Scarlata C, Sluiter J, Templeton D, Crocker D (2008) Determination of structural carbohydrates and lignin in biomass. Lab Anal Proced 1617:1–16
Tai H, Chang C, Cai W, Lin J, Huang S, Lin Q, Yuan E, Li S, Lin Y, Chan J, Tsao C (2023) Wood cellulose microfibrils have a 24-chain core-shell nanostructure in seed plants. Nat Plants 9:1154–1168
Tao W, Duan W, Liu C, Zhu D, Si X, Zhu R, Oleszczuk P, Pan B (2020a) Formation of persistent free radicals in biochar derived from rice straw based on a detailed analysis of pyrolysis kinetics. Sci Total Environ 715:136575
Tao W, Yang X, Li Y, Zhu R, Si X, Pan B, Xing B (2020b) Components and persistent free radicals in the volatiles during pyrolysis of lignocellulose biomass. Environ Sci Technol 54:13274–13281
Tao W, Zhang P, Yang X, Li H, Liu Y, Pan B (2021) An integrated study on the pyrolysis mecanism of peanut shell based on the kinetic analysis and solid/gas characterization. Bioresource Technol 329:124860
Tu R, Sun Y, Wu Y, Fan X, Cheng S, Jiang E, Xu X (2022) The fuel properties and adsorption capacities of torrefied camellia shell obtained via different steam-torrefaction reactors. Energy 238:121969
Van de Velden M, Baeyens J, Brems A, Janssens B, Dewil R (2010) Fundamentals, kinetics and endothermicity of the biomass pyrolysis reaction. Renew Energy 35:232–242
Wang Z, Huang C, Zhong J, Wang Y, Tang L, Li B, Sheng J, Chen L, Sun S, Shen X (2021) Valorization of Chinese hickory shell as novel sources for the efficient production of xylooligosaccharides. Biotechnol Biofuels 14:226

Wang W, Lemaire R, Bensakhria A, Luart D (2022) Review on the catalytic effects of alkali and alkaline earth metals (AAEMs) including sodium, potassium, calcium and magnesium on the pyrolysis of lignocellulosic biomass and on the co-pyrolysis of coal with biomass. J Anal Appl Pyrol 163:105479

Wang R, Yang J, Fu Z, Hu Y (2025) Thermal analysis of the pyrolysis characteristics of wet and dry biomasses from different forest layers. Biomass Convers Biorefin 15:31029–31044

Yang C, Quan Z, Chen Y, Zhu Q, Wang J, Li X (2020) A comprehensive investigation of the pyrolysis effect on heat transfer characteristics for *n*-Decane in the horizon mini-channel. Energy Fuels 34:199–210

Zhao D, Shu S, Zhao J, Liang Y, Wang H, Liu H, Li L, Wang D (2023) Interactions of H_2O and O_2 with char during gasification in mixed atmosphere analyzed by isotope tracer method and in-situ DRIFTS. Fuel 337:127173

Zitting A, Paajanen A, Altgen M, Rautkari L, Penttila PA (2024) Role of lignin in moisture interactions of cellulose microfibril structures in wood. Small Struct 5:2400167